Hydrogel delivery of lysostaphin eliminates orthopedic implant infection by *Staphylococcus aureus* and supports fracture healing

Christopher T. Johnson[a,b], James A. Wroe[a,b], Rachit Agarwal[b,c,1], Karen E. Martin[b,c], Robert E. Guldberg[b,c], Rodney M. Donlan[d], Lars F. Westblade[e], and Andrés J. García[b,c,2]

[a]Wallace H. Coulter Department of Biomedical Engineering, Georgia Institute of Technology and Emory University School of Medicine, Atlanta, GA 30332; [b]Petit Institute for Bioengineering and Bioscience, Georgia Institute of Technology, Atlanta, GA 30332; [c]Woodruff School of Mechanical Engineering, Georgia Institute of Technology, Atlanta, GA 30332; [d]Clinical and Environmental Microbiology Branch, Division of Healthcare Quality Promotion, Centers for Disease Control and Prevention, Atlanta, GA 30333; and [e]Pathology and Laboratory Medicine, Weill Cornell Medicine, New York, NY 10065

Orthopedic implant infections are a significant clinical problem, with current therapies limited to surgical debridement and systemic antibiotic regimens. Lysostaphin is a bacteriolytic enzyme with high antistaphylococcal activity. We engineered a lysostaphin-delivering injectable PEG hydrogel to treat *Staphylococcus aureus* infections in bone fractures. The injectable hydrogel formulation adheres to exposed tissue and fracture surfaces, ensuring efficient, local delivery of lysostaphin. Lysostaphin encapsulation within this synthetic hydrogel maintained enzyme stability and activity. Lysostaphin-delivering hydrogels exhibited enhanced antibiofilm activity compared with soluble lysostaphin. Lysostaphin-delivering hydrogels eradicated *S. aureus* infection and outperformed prophylactic antibiotic and soluble lysostaphin therapy in a murine model of femur fracture. Analysis of the local inflammatory response to infections treated with lysostaphin-delivering hydrogels revealed indistinguishable differences in cytokine secretion profiles compared with uninfected fractures, demonstrating clearance of bacteria and associated inflammation. Importantly, infected fractures treated with lysostaphin-delivering hydrogels fully healed by 5 wk with bone formation and mechanical properties equivalent to those of uninfected fractures, whereas fractures treated without the hydrogel carrier were equivalent to untreated infections. Finally, lysostaphin-delivering hydrogels eliminate methicillin-resistant *S. aureus* infections, supporting this therapy as an alternative to antibiotics. These results indicate that lysostaphin-delivering hydrogels effectively eliminate orthopedic *S. aureus* infections while simultaneously supporting fracture repair.

infection | biomaterials | orthopedics | lysostaphin | *S. aureus*

Orthopedic disease and injuries often require biomaterial implant and devices for successful clinical treatment. In 2011, 1.2 million prosthetic joint arthroplasty procedures were performed in the United States, and this number is projected to increase to 3.8 million procedures by 2030 (1). Infection of these devices is a major limitation with ineffective treatment options (2). For example, over 1 million joint prostheses (3) and 6 million fracture-fixation devices (4) are deployed each year, with 2% and 5% of these procedures, respectively, developing infection at an economic cost of over $2 billion (5). In the United States, 112,000 orthopedic device-related infections occur annually, with ~66% of these bacterial infections involving *Staphylococcus* species (6). Fracture fixation devices have infection rates ranging from 1 to 2% for closed fractures and rates as high as 30% for open fractures (7). Orthopedic implant infection occurs through three routes: direct contamination of the implant, infection spreading to the implant from a nearby source, and implant infection due to transient bacteremia, leading to implant colonization. Clinically, implant infections are primarily prevented by administration of antibiotics, the placement of antibiotic-laden bone cements, and the use of minimally invasive surgical techniques

(6). Current treatment of orthopedic implant infections is limited to a combination of aggressive surgical debridement, device removal, and long-term systemic antibiotic regimens. Antibiotic treatment can lead to the development of opportunistic infections through perturbations to the gut microbiota (8) and the development of antibiotic resistance (9). Further complicating the scenario is the formation of bacterial biofilms, populations of sessile and slowly dividing bacteria encapsulated within extracellular polymeric substances (10, 11). The biofilm matrix provides significant protection from the host immune system and acts as a diffusion barrier for antibiotics, allowing for bacteria to be resistant to antibiotic concentrations 1,000 times higher than that required to kill the same planktonic strain (12). Bacteria in biofilms can be exposed to subinhibitory antibiotic concentrations, further driving the development of antibiotic resistance (9). As such, current treatment strategies for device-related infections are significantly limited, often requiring one to two revision surgeries,

Significance

Orthopedic implant infections require long-term antibiotic therapy and surgical debridement to successfully retain the implant; however, therapeutic failure can lead to implant removal. Here an injectable PEG-based hydrogel that adheres to exposed tissue and fracture surfaces is engineered to deliver the antimicrobial enzyme lysostaphin to infected, implant-fixed, mouse femoral fractures. Lysostaphin encapsulation within the hydrogel enhances enzyme stability while providing enhanced antibiofilm activity and serving as a controlled delivery platform. In a preclinical animal model of orthopedic-implant infection, we show that lysostaphin-delivering hydrogels outperform prophylactic antibiotic therapy and soluble lysostaphin, by eradicating infection while promoting bone repair. Importantly, lysostaphin-delivering hydrogels are effective against antibiotic-resistant infections. This lysostaphin delivery platform could be highly effective at treating and preventing implant infections.

and causing significant patient morbidity, at a high economic cost of over $50,000 per case (6).

The widespread emergence of antibiotic-resistant bacteria is a growing public health threat, leading to a postantibiotic era, where current therapies are no longer effective (13). This threat has prompted the investigation of alternative strategies to traditional systemic antibiotic therapy. Lysostaphin is a 27-kDa antimicrobial enzyme with activity specific to *Staphylococcus* species (14). The enzyme has two domains, a cell wall-targeting domain, responsible for its specificity, and a lytic domain that cleaves the pentaglycine cross-bridges present in the bacterial cell wall (i.e., peptidoglycan) (15). Lysostaphin exhibits activity against antibiotic-resistant *Staphylococcus aureus* strains, including methicillin-resistant *S. aureus* (MRSA), vancomycin-intermediate *S. aureus*, vancomycin-resistant *S. aureus* (16–18), and *Staphylococcus epidermidis* (19). Importantly, lysostaphin kills planktonic and quiescent bacteria as well as cells growing in a biofilm (20), in contrast to most antibiotics that require active cellular metabolism to be effective (21). Widespread resistance to lysostaphin has not been reported from clinical samples (22), although several isolates have been generated in laboratory settings (23, 24). Additionally, the specificity of lysostaphin allows for only offending staphylococcal species to be eliminated, thus preventing adverse effects of gut microbiota perturbation, which is associated with systemic antibiotic therapy. These characteristics make lysostaphin an ideal candidate to treat infections primarily limited to *Staphylococcus* species and where biofilm formation is often implicated in the disease process (25). Lysostaphin has been delivered topically, systemically, or as material coatings in several small animal models to target *S. aureus* infections (18, 26–28). In humans, topical application of lysostaphin reduces *S. aureus* nasal carriage 5 d after treatment with no reported toxicity (29). Additionally, parental administration in a human patient has been reported without major side effects (30).

Despite these attributes, lysostaphin therapy has been severely limited by the lack of effective delivery vehicles. Conjugation of PEG to lysostaphin increases the in vivo half-life of systemically administered enzyme from less than 1 h to up to 24 h, but at the expense of reduced enzymatic activity (31). Biomaterial carriers have focused on surface conjugation of lysostaphin to a material to prevent bacterial colonization (28, 32–34), as opposed to developing enzyme delivery vehicles. Localized delivery of antimicrobial therapeutics allows for higher drug concentrations to be achieved at the infection site over a longer period of time, with a lower risk of toxicity compared with systemic delivery (35, 36). Hydrogels are water-swollen polymer networks that exhibit significant therapeutic versatility for localized protein delivery (37). We previously engineered injectable PEG-based hydrogels for controlled delivery of protein- and cell-based therapeutics (38–44). In this platform, four-arm PEG macromers functionalized with terminal maleimide groups (PEG-4MAL) that react specifically with thiols are functionalized with cell adhesive peptides and cross-linked into a network using thiolated molecules such as protease-degradable peptides with terminal cysteines. These synthetic hydrogels exhibit significant advantages over other delivery vehicles including well-defined composition and structure, minimal toxicity, stoichiometric incorporation of biomolecules, controlled polymerization kinetics, and nontoxic degradation products that are excreted in the urine (41, 42).

Here, we engineered lysostaphin-delivering injectable hydrogels to treat *S. aureus* orthopedic implant infections and support fracture repair (Fig. 1A). We characterized the activity, stability, and release of hydrogel-encapsulated lysostaphin, as well as antimicrobial and antibiofilm performance. The efficacy of lysostaphin-delivering hydrogels was tested in vivo using a murine femur fracture infection model. Bacterial reduction, cytokine profiling, and functional healing were measured to assess the therapeutic potential of lysostaphin-delivering hydrogel therapy. Finally, the antimicrobial efficacy of lysostaphin-delivering hydrogels against antibiotic-resistant bacteria was tested.
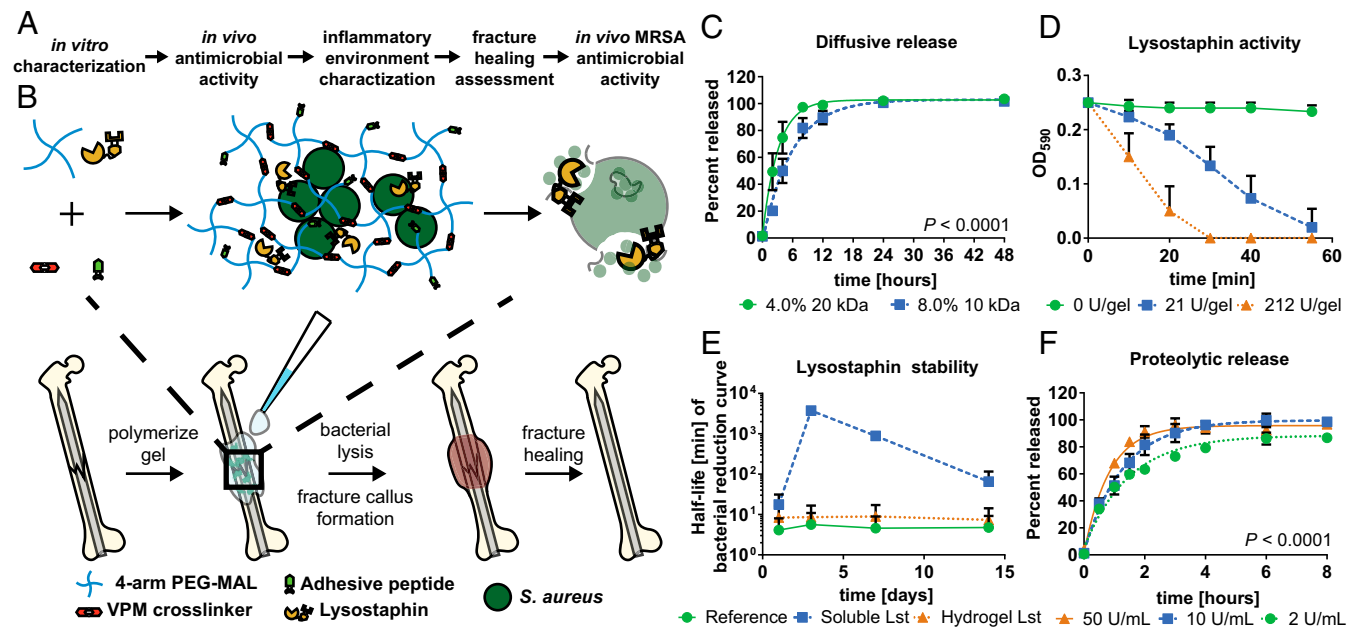
Fig. 1. Lysostaphin-delivering hydrogel synthesis and characterization. (*A*) Outline of overall study design. (*B*) Schematic diagram of lysostaphin encapsulation within protease-degradable PEG-MAL hydrogel and subsequent application to infected femurs, which leads to fracture callus formation and healing. (*C*) Passive lysostaphin release with one-phase association fit with extra sum of squares *F* test to compare *K* values are different. (*D*) Optical density curves of lysostaphin-laden hydrogels placed in *S. aureus* UAMS-1 suspensions as a function of incubation time. (*E*) Lysostaphin activity as measured by the average half-life of the kinetic bacteria reduction assay (*SI Appendix*, Fig. S3 *A–D*) at 1, 3, 7, and 14 d after hydrogel polymerization. (*F*) Protease-triggered release of lysostaphin with one-phase association fit using extra sum of squares *F* test to compare all *K* values are different. Lst, lysostaphin. Mean ± SD, *n* = 3–5.

Results

Encapsulation of Lysostaphin Within Injectable PEG Hydrogels Maintains Activity.

Orthopedic fractures range from simple closed fracture patterns with minimal soft tissue injury to complex open compound fractures with significant muscle injury, making delivery by injection and in situ polymerization desirable features in an antimicrobial delivery system. This property allows for the material to adhere to exposed tissue and fracture surfaces, ensuring local delivery to the injury. We synthesized PEG hydrogels in a one-step reaction by mixing PEG-4MAL macromers with the protease-degradable peptide cross-linker GCRDVPMSMRGGDRCG (VPM) (45) and cell adhesive peptides (e.g., RGD and GFOGER), which were covalently incorporated into the network by terminal cysteine groups that react specifically with maleimides on the PEG-4MAL macromer (Fig. 1*B*). Lysostaphin enzyme was physically entrapped within the hydrogel without covalent incorporation onto the polymer network due to the lack of free thiol groups in the protein (46). This injectable format allows for lysostaphin to maintain its activity throughout the hydrogel synthesis process. Sustained release of lysostaphin, both via passive diffusion through the hydrogel network and protease-dependent degradation of the hydrogel, results in lysis of target bacteria and supports bone formation and subsequent fracture repair (Fig. 1*B*). To assess the effect of hydrogel mesh size on diffusion-dependent release of lysostaphin, we labeled lysostaphin with a fluorescent dye (*SI Appendix*, Fig. S1) and measured its diffusion out of the hydrogel. Exponential one-phase association curves were then fit to these data. We synthesized hydrogels using different-sized PEG-4MAL macromers (10 kDa and 20 kDa) at 8.0% and 4.0% wt/vol to generate hydrogels with different mesh sizes. These PEG-4MAL macromers are chemically equivalent, except for the arm length, allowing for modulation of the hydrogel mesh size, thereby allowing for control of lysostaphin diffusion from the hydrogel. The 20-kDa hydrogels with a relatively larger mesh size exhibit more rapid lysostaphin release compared with the 10-kDa hydrogels with a tighter mesh structure (Fig. 1*C*). This result shows that as the mesh size is reduced the rate of diffusion-mediated release of lysostaphin is decreased. Both hydrogel formulations fully released all of the encapsulated lysostaphin within the first 24 h of swelling. Lysostaphin release could be prolonged by further reducing the hydrogel mesh size, or by engineering a free cysteine into the lysostaphin protein, allowing for covalent tethering into the hydrogel. We also assessed the activity of the released lysostaphin after 24 h of swelling by assaying the swelling supernatant for lysostaphin activity, which showed that the released enzyme retained 50% activity after release from the hydrogel (*SI Appendix*, Fig. S2). To evaluate lysostaphin activity following encapsulation and release, hydrogels were synthesized and placed in a bacterial suspension of *S. aureus* UAMS-1, a clinical isolate from a pediatric case of osteomyelitis (47), and reduction of bacteria was monitored over time by optical density measurements. In this experiment, no protease was included so lysostaphin is released from the hydrogel only by diffusion. Lysostaphin-containing hydrogels rapidly and completely reduced bacteria levels in suspension (Fig. 1*D*). Importantly, the rate of bacterial clearance was dependent on the dose of encapsulated lysostaphin. Retention of enzyme activity after hydrogel polymerization is a critical design criterion. We assessed the long-term activity of lysostaphin encapsulated within the hydrogel carrier and compared it to enzyme maintained in solution and fresh, reference lysostaphin. Hydrogels were synthesized with lysostaphin and not swollen to prevent loss of enzyme to directly assess the hydrogel's capacity to maintain enzyme stability. Enzyme activity was determined by calculating the rate of bacterial killing, as defined by the time required to kill 50% of a UAMS-1 bacterial suspension. The rate of bacterial killing was determined by fully degrading the hydrogels in protease and immediately incubating this product with bacteria, then monitoring the reduction in optical density

over the course of 1 h (*SI Appendix*, Fig. S3). A one-phase decay curve was then fit to these data to obtain the half-life metric. Remarkably, hydrogel encapsulation preserved lysostaphin activity over 14 d when kept at 25 °C compared with soluble unencapsulated lysostaphin, which rapidly degraded (Fig. 1*E*). There was no difference in lysostaphin activity between hydrogel-encapsulated enzyme throughout 14 d and fresh enzyme.

Bacterial infection often triggers an inflammatory response, including locally elevated protease levels (48). The inclusion of protease-degradable peptide cross-links in lysostaphin-delivering hydrogels allows for lysostaphin to be released on-demand in response to infection and local protease activity. Protease-dependent release of lysostaphin was characterized by monitoring the release of fluorescently labeled lysostaphin from lysostaphin-laden hydrogels (20 kDa, 4.0% wt/vol) exposed to different levels of protease (Fig. 1*F*). The results show that higher levels of protease cause faster lysostaphin release, indicating protease-responsive release. Importantly, nearly all of the loaded enzyme was released in these assays. Measurement of the mechanical properties of lysostaphin-delivering hydrogels reveals that the addition of lysostaphin does not affect the elastic or viscous properties of the hydrogel, as determined by measuring the storage and loss moduli of the gels, respectively (*SI Appendix*, Fig. S4).

Encapsulated Lysostaphin Kills Bacteria, Including in Biofilms.

Lysostaphin is highly active against both *S. aureus* and *S. epidermidis* (20). We examined the bactericidal activity of the enzyme encapsulated in the hydrogel delivery system. Hydrogels were synthesized with different strains of *S. aureus* (Xen29, UAMS-1, and 46106) or *S. epidermidis* (IDRL-8883, a clinical strain isolated from a prosthetic joint infection) trapped within the hydrogel matrix with or without lysostaphin (*SI Appendix*, Table S1). The gels were then cultured overnight in bacterial growth media and after 24 h were assayed for viable bacteria. Encapsulated lysostaphin reduced viable bacteria to undetectable levels for all bacterial strains tested (Fig. 2 *A–D*). After confirming that lysostaphin-laden hydrogels are effective against various strains of bacteria, we tested the in vitro cytocompatibility of lysostaphin using human mesenchymal stem cells. We induced human mesenchymal stem cells to differentiate toward an osteogenic lineage and added lysostaphin to the culture media. Lysostaphin had no effects on the osteogenic differentiation of human mesenchymal stem cells as assessed by alkaline phosphatase activity (*SI Appendix*, Fig. S5*A*) and calcium deposition (*SI Appendix*, Fig. S5 *B* and *C*), demonstrating that lysostaphin effectively kills staphylococcal species but does not interfere with the osteogenic differentiation of human cells.

Orthopedic implant infections typically involve formation of a bacterial biofilm. The biofilm protects the bacteria from the host immune response and acts as a diffusion barrier for antibiotics, making them particularly difficult to eliminate. We evaluated the antibiofilm activity of lysostaphin-delivering hydrogels. We hypothesized that delivery via the hydrogel carrier would improve the antibiofilm activity of the enzyme compared with soluble enzyme alone based on our observation that encapsulation within the hydrogel prolonged enzyme stability (Fig. 1*C*). *S. aureus* strain UAMS-1 is a prolific biofilm former (49). We grew UAMS-1 biofilms for 24 h and then treated them with lysostaphin-laden hydrogels or soluble enzyme. After 18 h of treatment, bacterial reduction was assessed by staining for live bacteria and subsequently imaging the biofilm. Fig. 2*E* shows representative images of biofilms after treatment. There is a clear lysostaphin dose-dependent reduction in live bacteria for the hydrogel-treated group, which is confirmed by image quantification (Fig. 2*F*). Comparisons between equivalent concentrations of lysostaphin demonstrate that hydrogel-mediated delivery of lysostaphin significantly reduces bacteria compared with delivery without a carrier (Fig. 2*F*).

www.manaraa.com
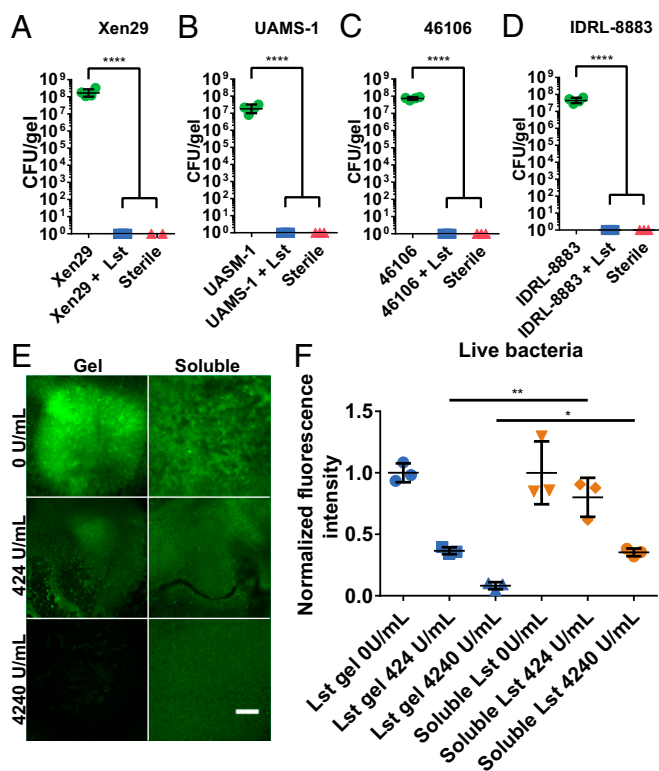
Fig. 2. Lysostaphin-laden hydrogels effectively kill bacteria in vitro. Bacterial counts reported as cfu per gel after 24 h of culture for (*A*) *S. aureus* Xen29, (*B*) *S. aureus* UAMS-1, (*C*) *S. aureus* 46106, and (*D*) *S. epidermidis* IDRL-8883. Mean ± SD, *n* = 3–4 per group. ****$P < 0.0001$, one-way ANOVA with Tukey's post hoc test. (*E* and *F*) Biofilms were generated by culturing UAMS-1 for 24 h statically and were then treated overnight with a hydrogel or soluble enzyme. (*E*) Images and (*F*) quantification of average image intensity of live bacteria after treatment. One-way ANOVA with Holm–Sidak's post hoc test between equivalent lysostaphin concentrations for hydrogel vs. soluble control. Mean ± SD, *n* = 3 per group. *$P < 0.05$, **$P < 0.01$. (Scale bar, 500 μm.)

Lysostaphin-Laden Hydrogels Effectively Reduce *S. aureus* Infection of Bone Fractures. Treatment of long bone fractures, such as the femur, often require fixation devices to stabilize the injury, enable healing, and promote return to mobility. However, bacterial infection of devices used to stabilize orthopedic injuries leads to the inability of fractures to heal, characterized by bone resorption, reactive bone formation, implant loosening, and, ultimately, device failure (2). To model this situation in vivo, we developed a mouse model of orthopedic implant infection. In this model, the femur is fractured using a custom three-point bending device; the fracture is then stabilized with a 25-gauge needle placed in the femoral shaft (50), and then a hydrogel is polymerized in situ over the fracture (Fig. 3*A*). Importantly, the injectable hydrogel formulation adheres to exposed tissue and fracture surfaces, ensuring efficient, local delivery. For mice receiving an infection, bacteria is mixed with the hydrogel components and polymerized in situ over the fracture. We then measure bacterial counts 1 wk after fracture or assess fracture healing 5 wk postimplantation.

Lysostaphin-delivering hydrogels should support fracture repair in the absence of infection to be an acceptable therapy for preventing staphylococcal infections. We hypothesized that the application of a lysostaphin-laden hydrogel would not impair normal (sterile) fracture healing. To test this, femoral fractures were treated with a sterile, lysostaphin-delivering hydrogel or left untreated. No bacteria were delivered in this experiment. After 5 wk, femora were explanted and analyzed by microcomputed

tomography (μCT), mechanical testing, and histology to evaluate fracture repair. μCT reconstructions revealed no gross morphologic differences in the fracture callus (*SI Appendix*, Fig. S6A). Similarly, no differences in fracture callus volume (*P* = 0.26, *SI Appendix*, Fig. S6B) or mechanical strength (*P* = 0.94, *SI Appendix*, Fig. S6C) of the repaired femora were detected between untreated and lysostaphin-delivering hydrogel-treated mice. Histological staining with H&E for tissue morphology and safranin-O and fast green (Saf-O/FG) for cartilage also showed no gross differences in healing between sterile control fractures and fractures treated with lysostaphin-delivering hydrogels (*SI Appendix*, Fig. S6D).

We next evaluated the ability of lysostaphin-delivering hydrogels to prevent *S. aureus* infection in vivo using the murine infected femur fracture model. Mouse femora were fractured and hydrogels containing methicillin-sensitive *S. aureus* UAMS-1 were polymerized in situ over the fracture to induce infection with or without lysostaphin. We included a group treated with soluble lysostaphin (no hydrogel) as well as an antibiotic prophylaxis group that received a single injection of oxacillin (100 mg/kg) preoperatively to directly compare the lysostaphin-delivering hydrogel to antibiotic-based therapy. Seven days postoperation, animals were killed, tissue was separated, and viable bacteria were enumerated in the tissue surrounding the femur (Fig. 3*B*), the femur (Fig. 3*C*), and the stabilization needle (Fig. 3*D*). Untreated infected controls had high numbers of recovered bacteria, indicating a persistent infection. Mice receiving prophylactic oxacillin therapy before the operation also had elevated bacteria counts, demonstrating that prophylactic antibiotic treatment did not prevent bacterial infection in this model. This result is consistent with clinical experience with systemic antibiotic regimens that do not consistently eliminate *S. aureus* infections (51). Treatment with lysostaphin-laden hydrogels significantly reduced the amount of recovered bacteria compared with the infection-only control and infections receiving systemic oxacillin. Importantly, the lysostaphin-laden hydrogels reduced bacteria counts to the same level as sterile controls. For the soluble lysostaphin-treated group, variable levels of bacteria were recovered and there was no difference in bacteria counts between this group and the infection-only control or the oxacillin-treated group, demonstrating that the hydrogel delivery vehicle is necessary to effectively treat these infections. Histologic analysis demonstrated significant leukocyte infiltration for infection-only and oxacillin-treated fractures compared with sterile fractures and fractures treated with lysostaphin-laden hydrogels (Fig. 3*E*). Saf-O/FG staining indicated poor collagen staining at the fracture site, characteristic of inhibited fracture repair, for the infection-only and oxacillin-treated fractures. In contrast, the lysostaphin-laden hydrogel-treated samples showed collagen deposition at the fracture site, consistent with the sterile control. Gram-positive bacteria were detected in the infection-only control and oxacillin-treated groups, showing that the infection persisted over the course of the experiment. We note that the sample shown from the highly variable soluble lysostaphin-treated group corresponds to a sample with no bacterial counts and as expected has features comparable to the sterile control and lysostaphin-delivering hydrogel sample. No gram-positive bacteria were detected in the lysostaphin-treated and sterile groups. Taken together, these results demonstrate that lysostaphin-delivering hydrogels eliminate *S. aureus* infections of bone fractures and outperform systemic antibiotic and direct delivery of soluble lysostaphin.

Lysostaphin Delivery to Infections Restores a Sterile Inflammatory Environment. Bone healing is characterized by three primary phases. The inflammatory phase is the initial step in the healing process, lasting approximately 1 wk, and is followed by the remodeling phase over the next 4–6 wk where the fracture callus is formed and mineralized. The final remodeling phase occurs

Johnson et al.

www.manaraa.com
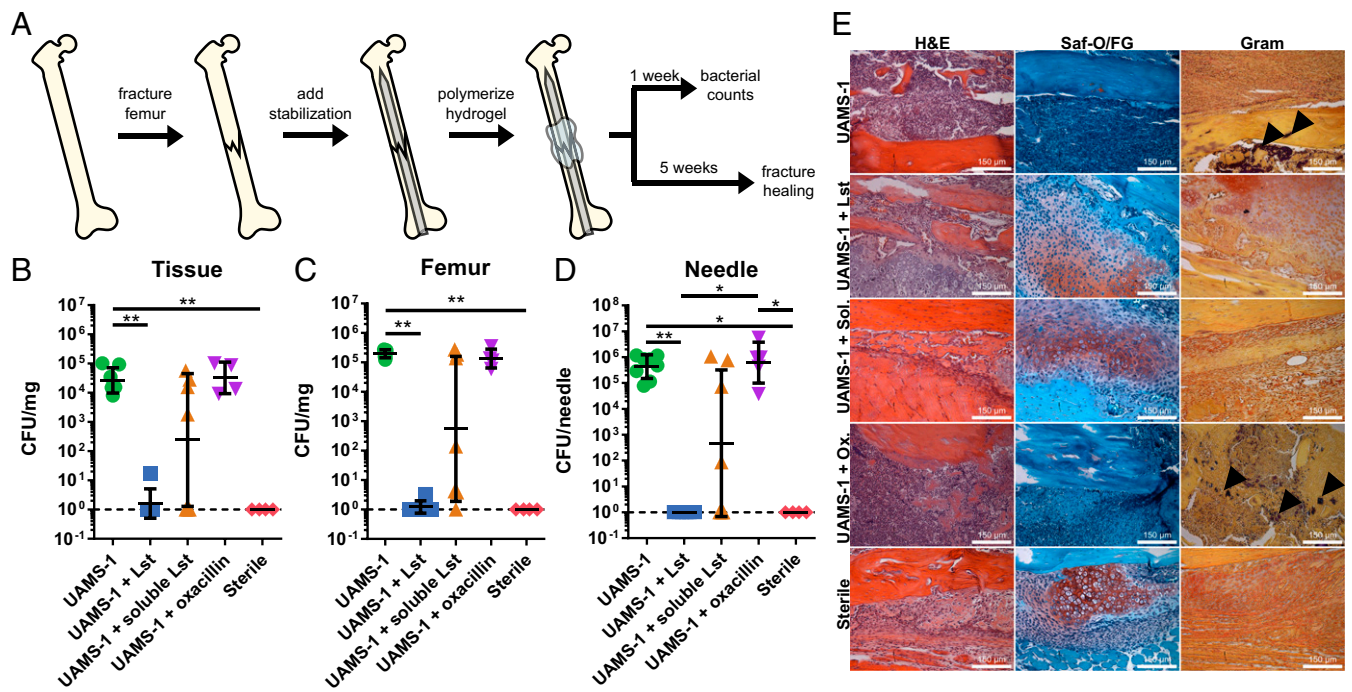
Fig. 3. Lysostaphin-delivering hydrogels eliminate bacteria in infected fractures. (*A*) Schematic diagram of mouse femur infection model. Quantification of *S. aureus* UAMS-1 recovered from the (*B*) tissue surrounding the femur, (*C*) femur bone, and (*D*) stabilization needle 7 d postfracture. Dashed line indicates detection limit. *$P < 0.05$, **$P < 0.01$. (*E*) Histological sections of femurs 7 d postfracture stained for H&E, Saf-O/FG, and Gram. Black arrows indicate gram-positive bacteria. Kruskal–Wallis test with Dunn's multiple comparisons test. Ox., oxacillin; Sol., soluble. Mean ± SD $n = 4$–8, compilation of four independent experiments.

over the next 3–6 mo, leading to complete fracture healing (52). This initial inflammatory phase is critical to successful fracture repair. A major concern of bactericidal therapy is an elevated and sustained inflammatory response to bacterial degradation products that negatively affects healing responses (10). Lysostaphin catalytically degrades the bacterial cell wall, leading to cell lysis and subsequent release of bacterial debris; the release of these bacterial products could cause a significant inflammatory response. To analyze this inflammatory response and assess the safety profile of lysostaphin therapy, we treated fractures with UAMS-1–infected hydrogels containing lysostaphin or empty hydrogels. Sterile hydrogels devoid of *S. aureus* UAMS-1 containing lysostaphin were included as the healing control. One week postinfection, we performed a multiplexed cytokine array assay on explanted tissue. Hierarchal cluster analysis using the Ward method revealed clear separation between the infected scaffolds and the sterile and lysostaphin-hydrogel–treated gels (Fig. 4*A*). Multivariate ANOVA with a sum combination across all cytokines demonstrated significant differences ($P < 0.001$) between the infection-only group and the sterile and lysostaphin-gel treated fractures (Fig. 4*B*). Importantly, significant overlap was observed between the sterile and lysostaphin-laden hydrogel groups, suggesting that the lysostaphin-delivering hydrogels restored the local inflammatory environment to a sterile state. Elevated levels of G-CSF, IL-1a, IL-1b, IL-6, KC, IP-10, MIP-1a, MIP-1b, and MIP-2 (Fig. 4 *C–K*), important cytokines in the inflammatory response to infection, were present in the UAMS-1–only group compared with the sterile control and lysostaphin-hydrogel–treated infections. No differences were detected between the sterile and lysostaphin hydrogel-treated groups for any of the cytokines. These results provide further evidence that lysostaphin-delivering hydrogels clear infecting bacteria and restore an inflammatory environment that could support fracture repair.

Lysostaphin-Delivering Hydrogels Result in Healing of Infected Femoral Fractures. To determine whether treatment of infections with lysostaphin-delivering hydrogels effectively reduces bacterial infection and promotes fracture repair, we assessed functional fracture healing at 5 wk postinfection. Mouse femora were fractured and hydrogels containing *S. aureus* UAMS-1 were placed at the fracture site to induce infection. These hydrogels contained lysostaphin or were left naïve as controls. The lysostaphin-delivering hydrogels were benchmarked against soluble lysostaphin delivery. Sterile, lysostaphin-delivering hydrogels were included as the positive healing control. The fractures were allowed to heal for 5 wk and then fracture repair was analyzed using μCT imaging, torsion to failure testing was used to assess the mechanical integrity of the femora, and histologic evaluation. Reconstructions of μCT scans (Fig. 5*A*) show no callus formation in the UAMS-1–infected control group and the presence of bone resorption and reactive bone formation around the fracture site, which is characteristic of osteomyelitis caused by bacterial infection. The sterile controls developed a robust fracture callus with evidence of bone remodeling, demonstrating fracture healing. All mice in the lysostaphin-laden hydrogel treated group showed significant fracture healing. A fracture callus was formed and the volume of the callus (Fig. 5*B*, $P > 0.99$) and bone deposition within the callus (Fig. 5*C*, $P > 0.99$) were equal to the sterile controls. Callus volume and bone volume were higher for infected fractures treated with lysostaphin-laden hydrogels compared with infection-only fractures ($P < 0.05$, Fig. 5 *B* and *C*). Fracture repair was highly variable in the soluble lysostaphin-treated group; two of six samples did not form a fracture callus and displayed features of osteomyelitis, including bone resorption and reaction bone formation (*SI Appendix*, Fig. S7*A*). The remaining four of six samples treated with soluble lysostaphin formed a fracture callus and progressed toward fracture healing (*SI Appendix*, Fig. S7*B*). Importantly, the torsional strength of infected fractures treated with lysostaphin-laden hydrogels was significantly higher than that for

www.manaraa.com
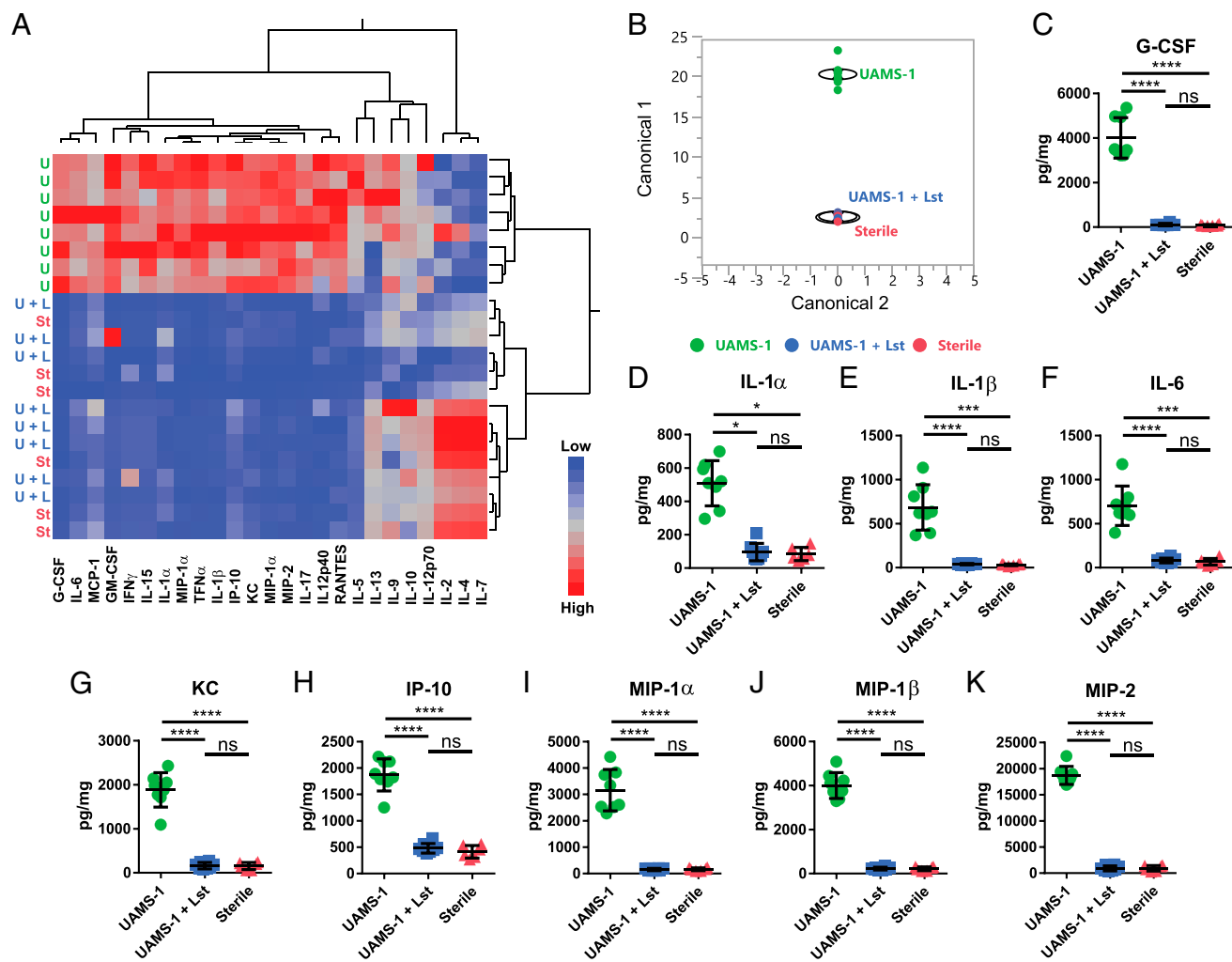
Fig. 4. Lysostaphin-laden hydrogel therapy restores a sterile inflammatory environment. Femora were fractured and infected with UAMS-1 and treated with hydrogels with or without lysostaphin and the inflammatory milieu of tissue at the fracture site 7 d postinfection was assessed using multiplexed cytokine analysis. (*A*) Hierarchical cluster analysis of cytokine profiles using the Ward method. (*B*) Multivariate-ANOVA plot using a sum combination across cytokines, $P < 0.001$. (*C–K*) Cytokines with statistically different tissue levels as determined using two-way ANOVA with a Bonferonni correction for multiple comparisons. U, UAMS-1; U + L, UAMS-1 + Lst; St, sterile. Mean ± SD, $n = 6–8$ per group. *$P < 0.05$, ***$P < 0.001$, ****$P < 0.0001$; ns, not significant.

the infection-only control ($P < 0.001$), and these high torque values were equivalent to those for the sterile control group (Fig. 5*D*). Bacterial counts performed at 5 wk postfracture (*SI Appendix*, Fig. S8) indicate that the infection persists and remains stable in the untreated infected controls over the 5-wk experimental time course and that lysostaphin-delivering hydrogel-treated mice remain sterile, confirming the results at 7 d postsurgery. Together, these data demonstrate that lysostaphin-delivering hydrogels clear the bacterial infection and support effective and complete fracture repair. No differences were observed between infected fractures treated with soluble lysostaphin and infection-only controls, again showing poor outcomes for lysostaphin therapy without the hydrogel carrier. Histologic sections of infected fractures treated with lysostaphin-delivering hydrogels and sterile fractures show no notable morphological differences (Fig. 5*E*), providing further support of successful fracture repair. The infection-only group shows significant leukocytic infiltrate on H&E staining and the presence of gram-positive bacteria (black arrows). The sample selected from the soluble lysostaphin treatment group shows the presence of gram-positive bacteria, indicating the sample was infected. This result clearly demonstrates persistent infection and inflammation for infected fractures that were not treated with

lysostaphin-laden hydrogel. Finally, as an initial assessment of the potential systemic toxicity of the lysostaphin-delivering hydrogels, serum liver enzyme tests and liver and kidney histology were performed at 5 wk postinfection. Liver enzyme testing revealed all values within the normal range (*SI Appendix*, Fig. S9), and no gross histological changes (*SI Appendix*, Fig. S10) were observed in the liver or kidney, supporting the safety of lysostaphin-delivering hydrogel therapy.

Lysostaphin-Delivering Hydrogels Clear MRSA Bone Infections. To test the efficacy of lysostaphin-delivery hydrogels to combat antibiotic-resistant bacteria, we measured bacterial numbers of the persistent infection at 7 d postoperation with the MRSA strain USA300. Mouse femora were fractured and hydrogels containing MRSA were placed at the fracture sites to induce infection. These hydrogels contained lysostaphin or were left empty as controls. Sterile lysostaphin-delivering hydrogels were used as controls. Consistent with the results obtained with UAMS-1, lysostaphin-delivering hydrogels significantly reduced MRSA bacteria counts compared with the infection-only control for the tissue surrounding the femur (Fig. 6*A*), the femur (Fig. 6*B*), and the stabilization needle (Fig. 6*C*). Notably, all of the

Johnson et al.

www.manaraa.com
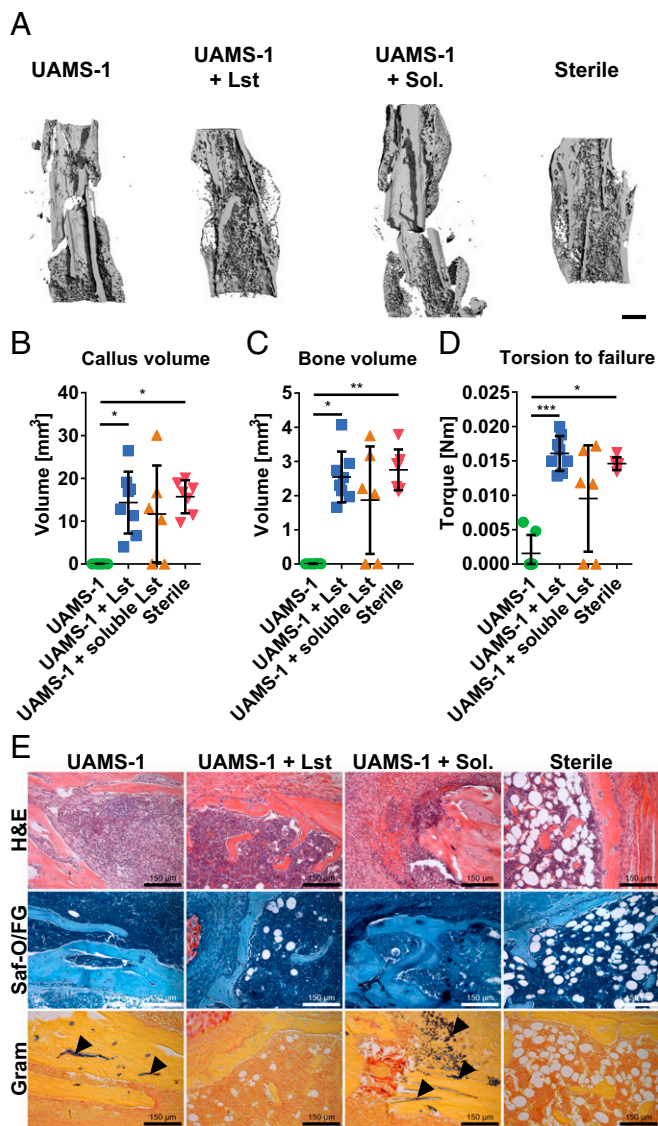
Fig. 5. Lysostaphin-delivering hydrogels enable fracture healing. (*A*) μCT reconstructions of the fracture callus 5 wk postoperation. (Scale bar, 1 mm.) Quantification of μCT reconstructions showing the (*B*) fracture callus volume and (*C*) bone volume within the fracture callus at 5 wk. (*D*) Mechanical strength of femurs as assessed by ex vivo torsion to failure testing. *$P < 0.05$, **$P < 0.01$, ***$P < 0.001$. (*E*) H&E, Saf-O/FG, and Gram staining of femurs. Black arrows indicate gram-positive bacteria. Kruskal–Wallis test with Dunn's multiple comparisons test. Mean ± SD, $n = 6$–8, compilation of two independent experiments.

lysostaphin hydrogel-treated mice had undetectable levels of bacteria. This shows that lysostaphin-delivering hydrogels eradicate antibiotic-resistant bacteria.

Discussion

Orthopedic implant infections are a significant clinical problem and lack effective therapies. Current interventions are limited to long-term systemic antibiotics, surgical debridement, and implant removal. Alternative therapy with antimicrobial enzymes such as lysostaphin provides for effective killing of specific bacterial species; however, these approaches are limited by the lack of suitable delivery vehicles. Here, we engineered synthetic hydrogels to deliver active lysostaphin to infected bone fractures to clear the infection and promote fracture healing. The synthetic hydrogel delivery vehicle maintained lysostaphin activity

over 14 d and controlled the release of active enzyme via passive and protease-triggered mechanisms. These hydrogels displayed high activity against various strains of *S. aureus*, as well as a methicillin-resistant *S. epidermidis* clinical isolate from a prosthetic joint infection in vitro. Importantly, lysostaphin delivery via the hydrogel carrier outperformed soluble enzyme when treating biofilms, most likely due to the sustained release of active lysostaphin. In a murine model of fracture infection, lysostaphin-delivering hydrogels cleared the infections and supported fracture repair, with bone formation and mechanical properties equivalent to those of uninfected fractures. Lysostaphin-delivering hydrogels restored the local inflammatory environment to that of sterile fractures at 7 d. In contrast, infected fractures treated with either prophylactic antibiotics or soluble lysostaphin showed no differences in bacterial levels and impaired healing compared with the infection controls. Notably, delivery of lysostaphin with this hydrogel carrier significantly reduced MRSA infections in this fracture model. Finally, no signs of liver toxicity or histologic changes to the liver or kidneys were observed for mice treated with lysostaphin-delivering hydrogels at 5 wk. Taken together, these results show that hydrogel-mediated delivery of lysostaphin eliminates fracture infections, including antibiotic-resistant strains, allowing for the endogenous fracture repair mechanisms to progress and healing to occur.

Biomaterial strategies to deliver active lysostaphin have primarily focused on surface functionalization, either by passive adsorption (27, 53), covalent tethering (33, 34), or impregnation within a coating (28, 54). This is an effective way to reduce bacteria at the material surface but may not be practical for settings where infection is already established, or not localized to a material surface (e.g., surrounding tissue). Our injectable formulation allows for in situ polymerization of the hydrogel at the fracture site, adhering to the exposed tissue and fracture surfaces, which is an important feature for treating complex fractures. We demonstrate that lysostaphin-delivering hydrogels have greater antibiofilm activity compared with soluble lysostaphin. This effect may be attributed to the enhanced enzyme stability and higher concentrations of lysostaphin localized to the biofilm achieved using the hydrogel carrier. Together, these material properties could allow for a broader application of lysostaphin-delivering hydrogels to treat other types of staphylococcal infections.

We demonstrate that lysostaphin-delivering hydrogels are effective at reducing infection for both clinical osteomyelitis and MRSA isolates in vivo. Importantly, we did not observe any lysostaphin resistance in our in vivo studies as *S. aureus* was effectively eradicated.
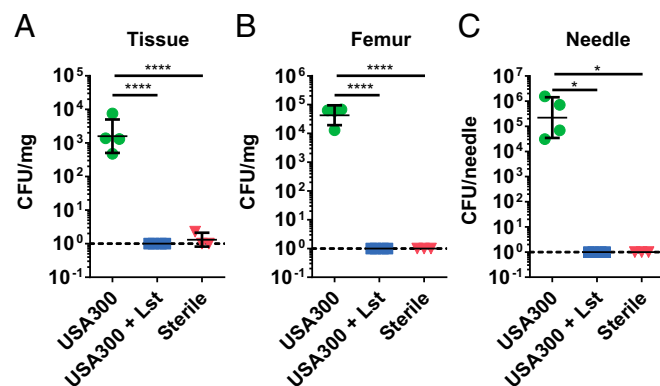
Fig. 6. Lysostaphin-laden hydrogels clear MRSA infections. Quantification of MRSA USA300 recovered from the (*A*) tissue surrounding the femur, (*B*) femur, and (*C*) stabilization needle at 7 d postfracture. Dashed line indicates detection limit. ANOVA with Tukey's post hoc test for *A* and *B*. Kruskal–Wallis test with Dunn's multiple comparisons test for *C*. Mean ± SD, $n = 3$–4. *$P < 0.05$, ****$P < 0.0001$.

www.manaraa.com

However, the development of resistance to the treatment is still a potential concern. Interestingly, lysostaphin exhibits synergism with β-lactam antibiotics, and lysostaphin exposure can sensitize strains to the antibiotic they have resistance against (19, 24). Therefore, lysostaphin delivery together with antibiotics could broaden the activity of the enzyme, while also reducing the chance of resistance developing. A lysostaphin-based approach offers several advantages over traditional small-molecule antibiotics. The bacteriospecific nature of lysostaphin provides specific targeting of the infecting organism, which may reduce complications associated with disrupting commensal bacteria (8). Small-molecule antibiotics primarily function through disruption of bacterial metabolic processes, leading to growth inhibition and death. This reliance limits drug activity against biofilm bacteria. The enzymatic nature of lysostaphin sidesteps this requirement, as the enzyme directly disrupts and kills bacteria. This feature contributes to the low concentrations (nanograms per milliliter range) required to kill bacteria compared with antibiotics (micrograms per milliliter range) (20), thereby reducing the amount of enzyme needed to provide bactericidal activity to the infection site.

Lysostaphin-delivering hydrogel treatment assists in restoring a prohealing inflammatory environment, supported by the absence of differences in cytokine secretion profiles compared with the sterile control. We attribute this effect to the kinetics of bacterial debris clearance by inflammatory cells, which is complete by 7 d after treatment. This result also supports the translation of lysostaphin therapy, as rapid bacterial killing and clearance are critical features for materials designed to treat infections. Importantly, lysostaphin administration with the hydrogel carrier eradicates the infection while supporting fracture healing as assessed by both μCT imaging and mechanical testing. The protease-degradable nature of the hydrogel carrier, in addition to protease-triggered release of lysostaphin, allows for host cells to degrade the hydrogel during repair, resulting in replacement of the gel with repair tissue. This is in contrast to nondegradable scaffolds that are either never removed or only removed at revision surgery once the infection is cleared. A concern with lysostaphin use is the development of neutralizing antibodies. Indeed, several studies have reported antibody development (29, 31, 55), but bacteriolytic activity was preserved in rabbits immunized to lysostaphin before therapy (55). Additionally, deimmunization of lysostaphin by removing protein recognized by T-cell epitopes reduces the likelihood of antibody generation (56, 57), which could eliminate concerns of systemic immune response to therapeutic delivery. We found that one of five mice treated with lysostaphin-delivering hydrogels tested positive for antilysostaphin IgG antibodies 5 wk after treatment, while none of the sterile or infected lysostaphin-free mice tested positive. However, preexposure serum was not tested for existing IgG titers, making it difficult to definitively conclude that the lysostaphin-delivering hydrogel generated an immune response. Furthermore, concerns over the development of neutralizing antibodies against lysostaphin are minimal for the bone repair application presented here as it would be exceedingly rare for a patient to have multiple independent infected or open fractures requiring lysostaphin therapy in a lifetime.

The present application focused on a biomaterial to specifically reduce *S. aureus* infections using lysostaphin. This technology could be further enhanced by broadening the antimicrobial spectrum to target other relevant pathogens in osteomyelitis cases, such as other coagulase-negative *Staphylococcus* species, *Pseudomonas,* and *Enterococcus* (6). Broadening the bacterial targets of the material will increase its utility as an effective prophylactic (58, 59). It will also be important to evaluate the ability to treat established biofilms in vivo (60). Species-specific antimicrobial therapies with activity toward bacteria growing in biofilm will help to successfully treat these complicated infections with reduced side effects to patients, such as disruption of the gut microbiota. Finally, this strategy will need to be evaluated in larger animal models for safety and efficacy to further assess its clinical potential.

Materials and Methods

Bacteria Strains and Culture. The bacteria strains used in these studies were UAMS-1 [ATCC 49230 (47)], USA-300 [ATCC BAA-1556 (61)], Xen29 [PerkinElmer (62)], 46,106 (CDC Clinical and Environmental Microbiology Branch Culture Collection), and IDRL-8883 [clinical isolate (63)] and are compiled in *SI Appendix*, Table S1. All strains were cultured on trypic soy agar (TSA) plates (BD Diagnostics) at 37 °C unless otherwise specified.

Preparation of Lysostaphin-Delivering Hydrogels. Twenty-kilodalton PEG-4MAL macromer (Lysan Bio) was mixed with recombinant lysostaphin protein (AMBI Products LLC) in 100 mM MES buffer, pH 5.5–6.0. Hydrogels were then cross-linked in a one-step reaction by combining PEG-lysostaphin with either the GFOGER peptide, GGYGGP(GPP)₅GFOGER(GPP)₅GPC (New England Peptide), or the RGD peptide, GRDGSPC (AAPPTEC), VPM cross-linker, GCRDVPMSMRGGDRCG (Genscript), and the bacterial suspension. Bacterial suspensions were prepared by picking individual colonies of bacteria grown on a TSA plate overnight and suspending them in Dulbecco's PBS supplemented with calcium and magnesium (PBS) to an optical density of 0.20 at 600 nm (MicroScan Turbidity Meter; Siemens) and then diluting this suspension 100-fold. The viable count for all bacterial inocula was determined by plate count on TSA medium. Unless otherwise noted the hydrogels were 4.0% wt/vol 20-kDa PEG-4MAL, 1 mM GFOGER, and 424 U/mL lysostaphin. The amount of VPM cross-linker added was determined stoichiometrically by matching the remaining maleimide groups after accounting for GFOGER or RGD incorporation. After mixing, the hydrogels were allowed to gel for 15 min in a humidified incubator at 37 °C and 5.0% CO_2 for in vitro studies or polymerized over the fracture for in vivo studies.

Lysostaphin Activity and Stability Assays. Lysostaphin was encapsulated within 25-μL sterile hydrogels (4.0% wt/vol 20-kDa PEG-MAL, 1 mM RGD, VPM, and 424 U/mL lysostaphin). The soluble lysostaphin group was 424 U/mL lysostaphin in an equivalent buffer to the hydrogel formulation in 25 μL aliquots. The reference lysostaphin group was prepared fresh from frozen at each time point. At 1, 3, 7, and 14 d, samples were incubated in 50 μL of 730 U/mL collagenase for 1 h at 37 °C and then 50 μL of each sample was assessed for activity by incubating with 150 μL UAMS-1 inoculum. The inoculum was prepared by culturing UAMS-1 overnight in brain heart infusion (BHI) broth with shaking at 37 °C, washing three times in 200 mM Tris·HCl, pH 8.0, by centrifugation, and adjusting the optical density to 0.25 at 600 nm (MicroScan Turbidity Meter; Siemens). Changes in optical density at 590 nm were measured using a HTS 7000 Plus plate reader (PerkinElmer) every minute for 1 h at 35 °C.

Lysostaphin Release from PEG Hydrogels. Amine groups on lysostaphin were fluorescently tagged using an AlexaFluor 488 dye conjugated to a 2-kDa PEG linker functionalized with an NHS ester (Nanocs). The reaction was performed in 100 mM $NaHCO_3$ buffer at pH of 8.3 at room temperature for 1 h with continuous mixing in the dark. Excess dye was removed from labeled protein using an AKTA Pure 25 (GE Healthcare) in combination with a Superdex 75 increase size-exclusion column (GE Healthcare) using PBS as the running buffer, at 4 °C. Labeled lysostaphin was incorporated in the hydrogel conditions tested: 4.0% wt/vol 20-kDa PEG-4MAL, 1 mM RGD, VPM and 8.0% wt/vol 10-kDa PEG-4MAL, 1 mM RGD, VPM. For the diffusion release study, hydrogels were polymerized, swollen in PBS, and incubated statically at 37 °C and 5.0% CO_2. For the protease-triggered release studies, 4.0% wt/vol 20-kDa PEG-4MAL, 1 mM RGD, VPM hydrogels were swollen in PBS supplemented with 2 U/mL, 10 U/mL, or 50 U/mL collagenase type 1 (Worthington) and incubated shaking at 200 rpm, 37 °C, and 5.0% CO_2. At each time point, the supernatant was sampled and read (488/530 excitation/emission) on a Synergy H4 (BioTek) plate reader. The measured fluorescence values were normalized to the fluorescence of PEG-4MAL/lysostaphin mixtures of the respective hydrogel condition.

Released Lysostaphin Activity Assay. Hydrogels were swollen for 24 h, after which the swelling supernatant was assayed for enzymatic activity. A detailed protocol is available in *SI Appendix, SI Materials and Methods*.

Measurement of Hydrogel Mechanical Properties. The mechanical properties of the hydrogels were measured using a stress-controlled rheometer. A detailed protocol is available in *SI Appendix, SI Materials and Methods*.

Human Mesenchymal Stem Cell Differentiation Potential and Calcium Deposition. Bone marrow-derived human mesenchymal stem cells were cultured in osteogenic differentiation media supplemented with lysostaphin. Alkaline phosphatase and calcium deposition were measured. A detailed protocol is available in *SI Appendix, SI Materials and Methods*.

Johnson et al.

In Vitro Antimicrobial Assessment of Lysostaphin Gels. The indicated bacterial strain was grown overnight on TSA at 37 °C. Bacterial cells were suspended in sterile PBS to an optical density to 0.20 measured at 600 nm (Microscan Turbidity Meter; Siemens). This suspension was then diluted 100× in 100 mM MES buffer and used as the inoculum. Hydrogels were synthesized (4.0% wt/vol 20-kDa PEG-MAL, 1 mM RGD, VPM, 424 U/mL lysostaphin), inoculated with the diluted bacterial culture, and incubated overnight in 25% trypic soy broth at 37 °C statically. Viable bacteria were enumerated by washing the hydrogels three times in PBS and degrading them in 365 U/mL collagenase Type 1 (Worthington) for 1 h. The degraded gels were serially diluted in PBS and 10 µL of each dilution was plated on TSA and grown overnight at 37 °C. Colony-forming units (cfu) were then enumerated.

Antibiofilm Activity of Lysostaphin Hydrogels. Biofilms were grown by inoculating 500 µL of BHI supplemented with 1% glucose (64) in a 48-well tissue culture plate with 20 µL of UAMS-1 cells picked from a TSA plate and suspended in PBS to an optical density to 0.20 measured at 600 nm. The biofilm was cultured 24 h at 37 °C statically. Biofilms were washed with PBS and 75 µL hydrogels (4.0% wt/vol 20-kDa PEG-MAL, 1 mM RGD, VPM, 0 U/mL, 424 U/mL, or 4,240 U/mL lysostaphin) were polymerized on top of the biofilm or hydrogel buffer with a matching amount of lysostaphin added to the well and incubated for 15 min at 37 °C, 5.0% CO_2 to allow for hydrogel polymerization. BHI media with 1% glucose was then added and biofilms were grown overnight at 37 °C. Biofilms were washed, fixed with 4.0% paraformaldehyde, and stained using LIVE/DEAD BacLight Bacterial Viability Kit (Thermo Fisher) per the manufacturer's instructions (65). A Nikon-C2 laser scanning confocal microscope using a 4× objective to acquire four images per well that were subsequently stitched together was used to image the biofilms. Live bacteria stained with SYTO9 were imaged using a 488-nm excitation laser in combination with a 525/50-nm filter. Live bacteria were quantified by measuring the average pixel intensity of a 2,656.37-µm × 2,657.37-µm selection of the image centered over the center of the well. Normalized fluorescence was computed by dividing the sample's average image fluorescence to the average untreated control for each treatment strategy (soluble or hydrogel).

Murine Femur Fracture Model. All animal procedures were performed in accordance with Institutional Care and Use Committee-approved protocols at the Georgia Institute of Technology. Male C57/B6 mice 10–12 wk old were housed with 12-h light/dark cycles and freely provided food and water. Mice were anesthetized under isofluorane (1.5% isoflurane delivered with 0.5 L/min O_2) and administered slow-release buprenorphine (1 mg/kg) to control pain post operatively. Fur on the right hind leg was removed by shaving followed by the application of depilatory cream. Animals receiving antibiotic injections were administered oxacillin (100 mg/kg) intraperitoneally. The skin was disinfected by swabbing with alcohol followed by chlorhexidine. A lateral incision was made over the femur and the muscle was blunt dissected to expose the femur. The patella was then dislocated and a sterile 25-gauge needle was inserted into the femur shaft and retracted. The femur was fractured at the mid-diaphysis with a custom-made three-point bender. Following fracture, the needle was positioned through the femur to stabilize the fracture and cut to an appropriate length. For animals receiving a hydrogel, 5 µL of the hydrogel was pipetted over the fracture site and allowed to polymerize. The average inoculum of UAMS-1 used in all studies was $1.55 \pm 0.51 \times 10^8$ cfu/mL, which correlated to ~1,500 cfu per mouse. The inoculum for the USA300 study was 3.43×10^8 cfu/mL, correlating to ~3,400 cfu per mouse. For animals receiving soluble lysostaphin, 5 µL of lysostaphin at a concentration equal to that of the hydrogel was pipetted over the fracture after the infection was initiated with a hydrogel containing bacteria. The muscle and patella were then sutured back into place and the wound was closed using wound clips. An X-ray image (MX-20 Radiology System, 23 kV, 15-s scan time; Faxitron) was taken to confirm proper insertion of the needle and stabilization of the femur. Mice were allowed to recover under a warming lamp until they were ambulatory.

Recovery of Bacteria from Tissue Samples. Mice were killed by CO_2 inhalation 7 and 35 d after surgery. Wound clips were removed and the skin on the right hind leg was sterilized with alcohol. A lateral incision was made over the femur and the needle was removed from the femoral shaft and placed in PBS. The femur and surrounding tissue were separated, weighed, and placed in PBS. All samples were kept on ice following dissection and removal. The tissue and femur samples were then homogenized via bead beating (femur: MP Biomedicals lysing matrix A, 2 × 40 s at 6 m/s; tissue: OPS Diagnostics 1.4-mm zirconium beads, 5 × 40 s at 6 m/s) using the FastPrep-24 (MP Biomedical). Following homogenization, single-cell bacterial suspensions were achieved by a series of water bath sonication (42 kHz, Model 2510; Branson Co.) sonicating, and vortexing steps (sonicate 10 min, vortex 30 s, sonicate 5 min, vortex 30 s, sonicate 30 s, vortex 30 s) (66). Homogenates were serially diluted, plated on

TSA, and incubated overnight at 37 °C. Colonies were enumerated, normalized to sample weight, and transformed using the formula cfu = $\log_{10}(1 + X)$ to avoid negative values. The detection limit was set at 10 colonies in the un-diluted sample to avoid false-positive results.

µCT and Mechanical Testing of Femurs. Five weeks postoperatively, mice were killed by CO_2 inhalation. The femur was dissected and the needle was removed. The femur was placed in gauze soaked in 0.9% wt/vol saline and frozen at −20 °C until further analysis. Samples were thawed under running deionized water and imaged using the µCT50 (Scanco Medical) at 55 kVp and 145 µA with a 0.5-mm filter and 300-ms integration time to achieve a 10-µm voxel size. Three-dimensional reconstructions were generated by segmenting the fracture callus from cortical bone and applying a Gaussian filter (sigma = 0.8, support = 1) and threshold value equivalent to 50% of intact cortical bone (50). Immediately after imaging, samples were mounted in potting blocks filled with Wood's metal and torsion to failure was assessed with an MRTP-0.2NM force transducer (Interface) interfaced with an ELF 3200 (Bose) mechanical testing system running WinTest7. A continuous ramp function of 3°/s was applied and the highest recorded torque value was reported. Femurs not able to be tested due to a lack of mechanical integrity were assigned a value of 0.

Dot Blot for Antilysostaphin Antibody Generation. A dot blot assay on serum samples was performed to detect host-antibody generation against lysostaphin. A detailed protocol is available in *SI Appendix, SI Materials and Methods*.

Liver Enzyme Testing. Five weeks postfracture, animals were killed by CO_2 inhalation. Blood was collected via cardiac puncture and a comprehensive blood chemistry panel was performed by Anatech Diagnostics on the serum samples.

Histology of Tissue Samples. At the designated time point, mice were killed by CO_2 inhalation. For femur samples, the skin was removed, the needle was carefully extracted from the femoral canal, and the entire femur and intact surrounding tissue were fixed in 10% neutral buffered formalin. Femur samples were then decalcified in formic acid. The kidneys and liver were excised and fixed in 10% neutral buffered formalin. All samples were then paraffin embedded and 5-µm sections were prepared. Samples were deparaffinized, rehydrated, and stained using H&E, Saf-O/FG, or Gram stain. Color images were acquired with a Nikon Eclipse E600 microscope using a Plan Fluor 20× objective (Nikon), Micropublisher 5.0 RTV (Q imaging) color camera, and Q-Capture software (Q imaging).

In Vivo Cytokine Analysis. One week postoperatively, mice were killed via CO_2 inhalation. The femur was dissected and the fracture site with surrounding tissue was removed and placed in radioimmunoprecipitation assay buffer. Samples were minced and placed on ice. Samples were sonicated for 10 s and debris was pelleted by centrifugation. The supernatant was passed through a 0.45-µm filter, snap-frozen in liquid nitrogen, and stored at −80 °C until analysis. A MilliPlex 25-plex mouse cytokine kit (Millipore Sigma) was used per the manufacturer's instructions to assay for tissue concentrations of G-CSF, GM-CSF, IFN-γ, IL-1α, IL-1β, IL-2, IL-4, IL-5, IL-6, IL-7, IL-9, IL-10, IL-12p40, IL-12p70, IL-13, IL-15, IL-17, IP-10, KC, MCP-1, MIP-1α, MIP-1β, MIP-2, RANTES, and TNF-α. Samples with measurements below the detection limit of the assay were reported as the detection threshold. Similarly, samples with values greater than the standard cure were reported as the maximum. All cytokines were normalized to the total protein content of the individual sample, which was determined using a bicinchoninic acid assay kit (Pierce by Thermo Fisher) per the manufacturer's instructions.

Statistics. Individual data points are plotted with a line representing the mean and error bars indicating the SD of the mean. Statistical significance ($P < 0.05$) was determined using the Student t test to evaluate two groups, ANOVA for multivariate groups with a Tukey post hoc test or a Hold–Sidak comparison between preselected groups, or a Kruskal–Wallis test with Dunn's post hoc test for nonparametric data. One-phase association curves were fit to the release data and an extra sum of squares F test as used to compare that K values were different. All calculations were performed using Prism (Graph-Pad). The multivariate analysis of multiplex cytokine data were performed using JMP Pro-13. Multivariate ANOVA with a sum combination was used to compare across cytokines. A two-way ANOVA with a Bonferroni correction was used to make comparisons between groups for individual cytokines with Prism (GraphPad).

Johnson et al.

www.manaraa.com

1. Berríos-Torres SI, et al.; Healthcare Infection Control Practices Advisory Committee (2017) Centers for disease control and prevention guideline for the prevention of surgical site infection, 2017. *JAMA Surg* 152:784–791.
2. Inzana JA, Schwarz EM, Kates SL, Awad HA (2016) Biomaterials approaches to treating implant-associated osteomyelitis. *Biomaterials* 81:58–71.
3. Maradit Kremers H, et al. (2015) Prevalence of total hip and knee replacement in the United States. *J Bone Joint Surg Am* 97:1386–1397.
4. Antoci V, Chen AF, Parvizi J (2017) 7.9 Orthopedic implant use and infection. *Comprehensive Biomaterials II*, ed Ducheyne P (Elsevier, Oxford), pp 133–151.
5. Darouiche RO (2004) Treatment of infections associated with surgical implants. *N Engl J Med* 350:1422–1429.
6. Campoccia D, Montanaro L, Arciola CR (2006) The significance of infection related to orthopedic devices and issues of antibiotic resistance. *Biomaterials* 27:2331–2339.
7. Trampuz A, Zimmerli W (2006) Diagnosis and treatment of infections associated with fracture-fixation devices. *Injury* 37(Suppl 2):S59–S66.
8. Guarner F, Malagelada JR (2003) Gut flora in health and disease. *Lancet* 361:512–519.
9. Viswanathan VK (2014) Off-label abuse of antibiotics by bacteria. *Gut Microbes* 5:3–4.
10. Bryers JD (2008) Medical biofilms. *Biotechnol Bioeng* 100:1–18.
11. Flemming HC, Wingender J (2010) The biofilm matrix. *Nat Rev Microbiol* 8:623–633.
12. Stewart PS, Costerton JW (2001) Antibiotic resistance of bacteria in biofilms. *Lancet* 358:135–138.
13. Roca I, et al. (2015) The global threat of antimicrobial resistance: Science for intervention. *New Microbes New Infect* 6:22–29.
14. Schindler CA, Schuhardt VT (1964) Lysostaphin: A new bacteriolytic agent for the Staphylococcus. *Proc Natl Acad Sci USA* 51:414–421.
15. Baba T, Schneewind O (1996) Target cell specificity of a bacteriocin molecule: A C-terminal signal directs lysostaphin to the cell wall of Staphylococcus aureus. *EMBO J* 15:4789–4797.
16. Climo MW, Patron RL, Goldstein BP, Archer GL (1998) Lysostaphin treatment of experimental methicillin-resistant Staphylococcus aureus aortic valve endocarditis. *Antimicrob Agents Chemother* 42:1355–1360.
17. Mohamed MF, Hamed MI, Panitch A, Seleem MN (2014) Targeting methicillin-resistant Staphylococcus aureus with short salt-resistant synthetic peptides. *Antimicrob Agents Chemother* 58:4113–4122.
18. Patron RL, Climo MW, Goldstein BP, Archer GL (1999) Lysostaphin treatment of experimental aortic valve endocarditis caused by a Staphylococcus aureus isolate with reduced susceptibility to vancomycin. *Antimicrob Agents Chemother* 43:1754–1755.
19. Kiri N, Archer G, Climo MW (2002) Combinations of lysostaphin with β-lactams are synergistic against oxacillin-resistant Staphylococcus epidermidis. *Antimicrob Agents Chemother* 46:2017–2020.
20. Wu JA, Kusuma C, Mond JJ, Kokai-Kun JF (2003) Lysostaphin disrupts Staphylococcus aureus and Staphylococcus epidermidis biofilms on artificial surfaces. *Antimicrob Agents Chemother* 47:3407–3414.
21. Kumar JK (2008) Lysostaphin: An antistaphylococcal agent. *Appl Microbiol Biotechnol* 80:555–561.
22. Gründling A, Missiakas DM, Schneewind O (2006) Staphylococcus aureus mutants with increased lysostaphin resistance. *J Bacteriol* 188:6286–6297.
23. Boyle-Vavra S, Carey RB, Daum RS (2001) Development of vancomycin and lysostaphin resistance in a methicillin-resistant Staphylococcus aureus isolate. *J Antimicrob Chemother* 48:617–625.
24. Climo MW, Ehlert K, Archer GL (2001) Mechanism and suppression of lysostaphin resistance in oxacillin-resistant Staphylococcus aureus. *Antimicrob Agents Chemother* 45:1431–1437.
25. Hogan S, et al. (2017) Potential use of targeted enzymatic agents in the treatment of Staphylococcus aureus biofilm-related infections. *J Hosp Infect* 96:177–182.
26. Dajcs JJ, et al. (2000) Lysostaphin treatment of methicillin-resistant Staphylococcus aureus keratitis in the rabbit. *Invest Ophthalmol Vis Sci* 41:1432–1437.
27. Kokai-Kun JF, Chanturiya T, Mond JJ (2009) Lysostaphin eradicates established Staphylococcus aureus biofilms in jugular vein catheterized mice. *J Antimicrob Chemother* 64:94–100.
28. Windolf CD, Lögters T, Scholz M, Windolf J, Flohé S (2014) Lysostaphin-coated titan-implants preventing localized osteitis by Staphylococcus aureus in a mouse model. *PLoS One* 9:e115940.
29. Quickel KE, Jr, Selden R, Caldwell JR, Nora NF, Schaffner W (1971) Efficacy and safety of topical lysostaphin treatment of persistent nasal carriage of Staphylococcus aureus. *Appl Microbiol* 22:446–450.
30. Stark FR, Thornsvard C, Flannery EP, Artenstein MS (1974) Systemic lysostaphin in man–Apparent antimicrobial activity in a neutropenic patient. *N Engl J Med* 291:239–240.
31. Walsh S, Shah A, Mond J (2003) Improved pharmacokinetics and reduced antibody reactivity of lysostaphin conjugated to polyethylene glycol. *Antimicrob Agents Chemother* 47:554–558.
32. Belyansky I, et al. (2011) The addition of lysostaphin dramatically improves survival, protects porcine biomesh from infection, and improves graft tensile shear strength. *J Surg Res* 171:409–415.
33. Miao J, et al. (2011) Lysostaphin-functionalized cellulose fibers with antistaphylococcal activity for wound healing applications. *Biomaterials* 32:9557–9567.
34. Yeroslavsky G, Girshevitz O, Foster-Frey J, Donovan DM, Rahimipour S (2015) Antibacterial and antibiofilm surfaces through polydopamine-assisted immobilization of lysostaphin as an antibacterial enzyme. *Langmuir* 31:1064–1073.
35. Johnson CT, Garcia AJ (2014) Scaffold-based anti-infection strategies in bone repair. *Ann Biomed Eng* 43:515–528.
36. ter Boo G-JA, Grijpma DW, Moriarty TF, Richards RG, Eglin D (2015) Antimicrobial delivery systems for local infection prophylaxis in orthopedic- and trauma surgery. *Biomaterials* 52:113–125.
37. Slaughter BV, Khurshid SS, Fisher OZ, Khademhosseini A, Peppas NA (2009) Hydrogels in regenerative medicine. *Adv Mater* 21:3307–3329.
38. Cruz-Acuña R, et al. (2017) Synthetic hydrogels for human intestinal organoid generation and colonic wound repair. *Nat Cell Biol* 19:1326–1335.
39. García JR, Clark AY, García AJ (2016) Integrin-specific hydrogels functionalized with VEGF for vascularization and bone regeneration of critical-size bone defects. *J Biomed Mater Res A* 104:889–900.
40. Lee TT, et al. (2015) Light-triggered in vivo activation of adhesive peptides regulates cell adhesion, inflammation and vascularization of biomaterials. *Nat Mater* 14:352–360.
41. Phelps EA, et al. (2012) Maleimide cross-linked bioactive PEG hydrogel exhibits improved reaction kinetics and cross-linking for cell encapsulation and in situ delivery. *Adv Mater* 24:64–70.
42. Phelps EA, Headen DM, Taylor WR, Thulé PM, García AJ (2013) Vasculogenic biosynthetic hydrogel for enhancement of pancreatic islet engraftment and function in type 1 diabetes. *Biomaterials* 34:4602–4611.
43. Shekaran A, et al. (2014) Bone regeneration using an alpha 2 beta 1 integrin-specific hydrogel as a BMP-2 delivery vehicle. *Biomaterials* 35:5453–5461.
44. Weaver JD, et al. (2017) Vasculogenic hydrogel enhances islet survival, engraftment, and function in leading extrahepatic sites. *Sci Adv* 3:e1700184.
45. Patterson J, Hubbell JA (2010) Enhanced proteolytic degradation of molecularly engineered PEG hydrogels in response to MMP-1 and MMP-2. *Biomaterials* 31:7836–7845.
46. Sabala I, Jonsson IM, Tarkowski A, Bochtler M (2012) Anti-staphylococcal activities of lysostaphin and LytM catalytic domain. *BMC Microbiol* 12:97.
47. Gillaspy AF, et al. (1995) Role of the accessory gene regulator (agr) in pathogenesis of staphylococcal osteomyelitis. *Infect Immun* 63:3373–3380.
48. Wolcott RD, Rhoads DD, Dowd SE (2008) Biofilms and chronic wound inflammation. *J Wound Care* 17:333–341.
49. Evans RP, Nelson CL, Bowen WR, Kleve MG, Hickmon SG (1998) Visualization of bacterial glycocalyx with a scanning electron microscope. *Clin Orthop Relat Res* 243–249.
50. Shekaran A, et al. (2014) The effect of conditional inactivation of beta 1 integrins using twist 2 Cre, Osterix Cre and osteocalcin Cre lines on skeletal phenotype. *Bone* 68:131–141.
51. Moriarty TF, et al. (2017) Orthopaedic device-related infection: Current and future interventions for improved prevention and treatment. *EFORT Open Rev* 1:89–99.
52. Kalfas IH (2001) Principles of bone healing. *Neurosurg Focus* 10:E1.
53. Shah A, Mond J, Walsh S (2004) Lysostaphin-coated catheters eradicate Staphylococcccus aureus challenge and block surface colonization. *Antimicrob Agents Chemother* 48:2704–2707.
54. Hathaway H, et al. (2017) Thermally triggered release of the bacteriophage endolysin CHAP_K and the bacteriocin lysostaphin for the control of methicillin resistant Staphylococcus aureus (MRSA). *J Control Release* 245:108–115.
55. Dajcs JJ, et al. (2002) Immunity to lysostaphin and its therapeutic value for ocular MRSA infections in the rabbit. *Invest Ophthalmol Vis Sci* 43:3712–3716.
56. Blazanovic K, et al. (2015) Structure-based redesign of lysostaphin yields potent antistaphylococcal enzymes that evade immune cell surveillance. *Mol Ther Methods Clin Dev* 2:15021.
57. Zhao H, et al. (2015) Depletion of T cell epitopes in lysostaphin mitigates anti-drug antibody response and enhances antibacterial efficacy in vivo. *Chem Biol* 22:629–639.
58. Raphel J, Holodniy M, Goodman SB, Heilshorn SC (2016) Multifunctional coatings to simultaneously promote osseointegration and prevent infection of orthopaedic implants. *Biomaterials* 84:301–314.
59. Goodman SB, Yao Z, Keeney M, Yang F (2013) The future of biologic coatings for orthopaedic implants. *Biomaterials* 34:3174–3183.
60. Inzana JA, Schwarz EM, Kates SL, Awad HA (2015) A novel murine model of established Staphylococcal bone infection in the presence of a fracture fixation plate to study therapies utilizing antibiotic-laden spacers after revision surgery. *Bone* 72:128–136.
61. Diep BA, et al. (2006) Complete genome sequence of USA300, an epidemic clone of community-acquired meticillin-resistant Staphylococcus aureus. *Lancet* 367:731–739.
62. Pribaz JR, et al. (2012) Mouse model of chronic post-arthroplasty infection: Noninvasive in vivo bioluminescence imaging to monitor bacterial burden for long-term study. *J Orthop Res* 30:335–340.
63. Park KH, Greenwood-Quaintance KE, Schuetz AN, Mandrekar JN, Patel R (2017) Activity of tedizolid in methicillin-resistant Staphylococcus epidermidis experimental foreign body-associated osteomyelitis. *Antimicrob Agents Chemother* 61:e01644-16.
64. O'Neill E, et al. (2007) Association between methicillin susceptibility and biofilm regulation in Staphylococcus aureus isolates from device-related infections. *J Clin Microbiol* 45:1379–1388.
65. Williams MM, et al. (2009) Structural analysis of biofilm formation by rapidly and slowly growing nontuberculous mycobacteria. *Appl Environ Microbiol* 75:2091–2098.
66. Fu W, et al. (2010) Bacteriophage cocktail for the prevention of biofilm formation by Pseudomonas aeruginosa on catheters in an in vitro model system. *Antimicrob Agents Chemother* 54:397–404.

ENGINEERING

APPLIED BIOLOGICAL SCIENCES

Johnson et al.

www.manaraa.com